Response to Reviewer #1

Antoon van Hooft, Stéphane Popinet, and Bas van de Wiel

June 2018

The authors thank the reviewer for taking his/her time to comment on the manuscript.

The article describes tests of an adaptive grid scheme in a single-column model for two ABL cases. The results are compared with a fixed-resolution version of the same model, and with various other models. This is an interesting study and the results are clearly presented. The quality of the adaptive scheme solutions is encouraging. While the overall scope of the research is limited, it presents a possible avenue for future adaptive GCM development. There are a few places where more detail and clarification would be helpful (described below). I recommend acceptance of this article pending minor revisions.

The authors agree with most points brought forward by the reviewer and we have therefore revised the manuscript accordingly. We hope that the manuscript is now more clear, and a point-by-point response is presented below. Also a PDF highlighting all the changes that were made with respect to the original manuscript is available.

In the model overview, it is stated that the grid refinement criteria are tuned based on trial and error. How sensitive is the scheme performance to the tuning? If this type of adaptive scheme is implemented in a full GCM, will different tunings be necessary at different heights, geographical regions, or seasons?

It is the authors opinion that a complete discussion on the meaning, interpretation and selection of the refinement criterion warrants a study of its own. This is in fact part of our continued research, and hence is considered to be outside the scope of the present work. However, we agree that it is an important part of the grid adaptation algorithm that forms the basis of the present work. Therefore we have revised the manuscript considerably and have extended the analysis that was formerly in the appendix and moved it to the main text. Here we share our views on the usage of the criterion and argue that is provides a convenient and consistent framework for finding a balance between accuracy and performance. The new figures also provide quantitative results on this topic. How to translate these results obtained for the Ekman-spiral case to an SCM/GCM is still not obvious.

Furthermore, at this moment we cannot give a conclusive answer to the question regarding a variable refinement criterion. The authors do not see a good reason to employ a variable refinement criterion in time and space. Such an approach would mean that similar processes would be resolved with different accuracy depending on their localization in space and time. Our (current) philosophy is that for consistent meshing a pre-defined wish for accuracy can and should dictate the mesh's resolution depending of the resolved physics. On the otherhand, the physical processes that are dominant for the statistics of interest may change, depending on the time and location. Then, in practice, the accuracy requirements may vary and this could be refelected in the refinement criterion.

p.2 Sec. 1, Line 17: Sentence starting "However, it is important..." is unclear and needs to be rewritten.

We hope the section on the concept of fractal scaling is more clear in the revised manuscript.

p.2 Sec. 1 Line 23: Sentence starting "This work departs..." makes it sound like this work uses different methods than Van Hooft (2018), yet the next page Line 25 suggests the opposite. This sentence needs to be modified to make the meaning clearer.

We hope the sentence in clear in the revised manuscript.

p.3 Sec. 2 Line 12: Could you state at least the nature of the surface fluxes parameter- ization (e.g. bulk flux). Which type of closures in Holtslag and Boville are you referring to?

Based on the reviewers comment, we have added a detailed description of the used closures in section 2 of the revised manuscript.

p.56 Sec. 3.2 : Could you add a little more qualitative description of this GABLS case? Were there clouds? Is it a surface driven convective BL? Is the wind shear significant or important?

We have added a short overview of general conditions as they are modelled by the GABLS2 scenario. (lines)

p.5 Sec. 3 Line 12: It would be good to reiterate here that each 'level of refinement' halves the local grid spacing.

We have re-iterated that in the revised manuscript.

p.5 Sec. 3 Line 21: Are you saying the differences are only minor compared the the LES spread, or only minor compared to the SCM model spread?

We have revised the sentence to be more clear. We hope to convey the message that our SCM results are relatively close to the LES-ensemble results compared to the SCM results presented by the participants pf the original GABLS1 SCM intercomparison. Taking the LES as the 'truth': Notice that the fidelity in our results is due to the good performing description of the mixing closure by England and McNider (1995) (eq. 1 / 5 and 10 , original/revised), for this particular case.

Figure 3a: Unlike most models, thetav in your solution has a negative slope in the boundary layer, more negative even than the one other plotted model with a negative slope. Is this slope also consistent with your fixed-grid solution? Is there something atypical about your SCM physics that would allow this?

Yes, this is a known feature of the to the used eddy-viscosity closure. Using this local description for turbulent transport, a gradient is always "needed" for vertical mixing. This is not a realistic feature and better closures that account for counter-gradient transport are available. We have added a remark on this feature in the revised manuscript. Next we show that this gradient is indeed a formulation-specific feature. Therefore, we re-plot our results alongside results from runs with a different value for the maximum mixing length ($l_b l$, see Eqs. 7 and 8 in the revised manuscript). The results are presented in the figure below. The default value for $l_b l$ was suggested in the reference literature and the used closures for transport are not the topic of our study. The figure also shows that the slope is not due to the usage of the grid adaptation algorithm (as was suggested by reviewer #2). In fact, the results for θ_v are within $0.2K$, which is much smaller than the difference with other models (up to multiple Kelvins). The used scripts to obtained these results or available and presented online (`www.basilisk.fr/sandbox/Antoonvh/GABLS2forrev1and2.c`). We choose not to add this analysis to the main text as it does not really add something new to the results or change the overall analysis of the manuscript. As all reviewers already agree: the results are encouraging.

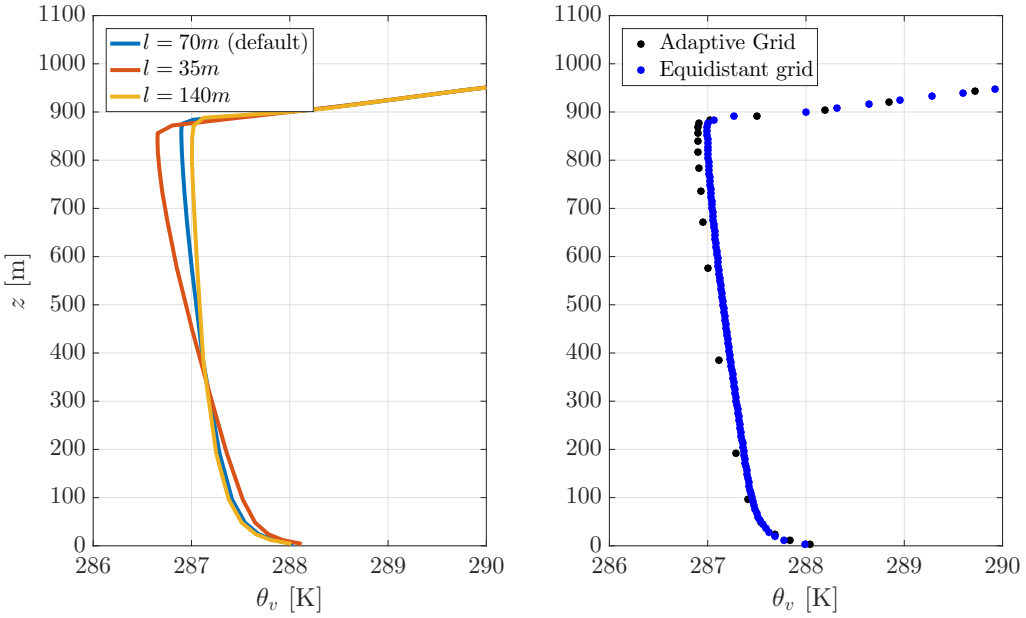

Figure 3c: What is the difference between the various shades of gray in the figure?

They are associated with different measurement techniques (see Svensson et al. (2011). Based on the reviewers comment we have stated this in the caption of this figure in the revised manuscript. Note that the forcings of for the GABLS2 case are idealized, and hence accuracy with respect to the measurements is not necessarily to be expected.

Figure 5 should have the simulation dates somewhere on the x-axis or at least the time coordinates referenced to a date in the caption.

We have added the date of the observation that inspired this (idealized) test case in the caption.

p. 6 Sec.3.2 Line 20: Stating that the evolution of the wind speed profile 'is the same' suggests that it is identical which is inaccurate. Perhaps 'is nearly the same'.

The reviewer is right and the sentence is revised accordingly in the new manuscript.

p. 6 Sec.3.2 Line 22: Could you clarify what is meant by 'Stullian image'? It would be helpful in this discussion if you qualitatively describe which parts of the diurnal cycle require the most/least refinement.

Since the conceptual evolution of a diurnal cycle of the ABL as presented in Stull (1991) (His fig. 1.7) is such a well known image, we hope to coin the term "Stullian image". This was done with permission of Roland Stull (private communication). The manuscript aims to describe qualitatively what parts of the ABL required grid refinement. This was infact the goal of bringing up the similarities with the image of Stull. Therefore, we have chosen to keep that discussion 'as is'.

Technical corrections:
p.1 Sec. 1 Line 3: 'receives' should be 'receive'
p.2 Sec.2 Line 18: 'have' should be 'has'
p.4 Sec.2 Line 10: 'trail' should be 'trial'
p.4 Sec.2 Line 28: is 'that' referring to equation 6?
p.5 Sec.2 Line 33: Would be clearer as 'Online links are provied in table 1.'
p.5 Sec.3 Line 23: 'Noting' should be 'Note'
p.6 Sec.3.2 Line 17: '22-th' should be '22nd'
p.6 Sec.3.2 Line 22: 'Fig. 2' should be 'Fig. 5'
p.7 Sec.4 Line 3: 'efficient' misspelled
Appendix: Line 13: Sentence starting 'Using a domain...' is not a complete sentence.
Appendix: Line 18: 'facilitate' misspelled
Appendix: Line 18: would be clearer as 'we diagnose the number of used cells...'
Appendix: Line 19: Sentence starting 'Were the adaptive grid results....' is not a com- plete sentence.
Appendix: Line 22: Should be 'This plot reveals' or 'These plots reveal'

We thank the reviewer again for his/her careful reading of the manuscript and hope to have corrected the manuscript according to the suggested technical changes. Except for the suggestion that 'online' refers to the 'link (to)' rather than the location of the case set-up files.

Response to Reviewer #2

Antoon van Hooft, Stéphane Popinet, and Bas van de Wiel

June 2018

The authors thank the reviewer for taking his/her time to comment on the manuscript.

A Basilisk 18-02-16 based adaptive grid scheme is employed and compared with an equal-distant high vertical resolution grid scheme in the same single-column atmospheric model for two land atmospheric boundary layer case studies. The diurnal variations of fine vertical structure near the bottom and the top of boundary layer is well captured using the adaptive grid scheme. Results are encouraging and clearly presented, which shows potential for future applications in global climate models. However the following major concerns are suggested to be addressed before acceptance for publication:

We are happy the reviewer find the results encouraging and hope to address the concerns in our point by point response and in the revised manuscript. A PDF highlighting the changes that were made is also provided as a supplement.

[1] In current state-of-art SCM/GCMs, more than 20s or more variables are involved in physical and chemical process simulations. It is necessary to state clearly the basic rule for selecting the refinement criteria and to show sensitivity test results. For example in this study, the refinement criteria are assigned only for winds and temperature. The specific humidity Q is also a key physical variable in the SCM simulation, but no criteria is assigned, why? and how a new Q refinement criteria influences the scheme ghost points and overall cell points searching? And how a Q refinement criteria influences the boundary layer diurnal cycle (particularly the boundary layer clouds) simulation?

The reviewer is right, finding a suitable mesh that strikes a balance between computational efficiency and accuracy of the diagnosed solution statistics is a challenge when performing numerical simulations. The challenge becomes even more prominent when statistics of over 20 variables need consideration. This is true for pre-tuned static anisotropic meshes, equidistant grids and we do not claim that the grid-adaptation algorithm lifts this burden from the model user either. Therefore, In the absence of a procedure for selecting mesh sizes for the static-grid approach (that typically also rely on trial-and-error, ad hoc testing and experience), the authors do not agree that the present (novel) approach should come with such guidelines. Especially when in practice, the grid (in)dependence of specific solution statistics is an arbitrary concept. More concretely: The SCMs in the original GABLS1 and GABLS2 intercomparison projects all use different meshes and similarly, a second (theorized) adaptive grid model could use different values for the refinement criteria to strike a different balance speed performance and numerical accuracy.

That said, the authors agree that the concept of the refinement criteria may raise new questions for modellers and currently warrants more study. Based on the reviewer's comments we made a serious effort to extend the analysis of the case that was formerly presented in the appendix (i.e. the laminar Ekman spiral), and we have included in it the main text. This new section (3.1), aims to exemplify for this simple case, what the effect is of tuning the refinement criterion, and argue that it provides a user-friendly, convenient and consistent framework for finding a balance between computational efficiency and accuracy. Note that it is not obvious how these results would translate to an SCM and at this moment in time, we feel that the "trial-and-error approach" is an accurate description of how the current refinement criteria values for the SCM were found.

The reviewer is also right that it would be wise to extend the algorithm to also consider the atmospheric moisture content when pushing the method towards more realistic/applied scenarios. Note that this can be readily done by changing a line of code in the case set-up. However, for the GABLS1 case there is no moisture and for the GABLS2 case, moisture only slightly modifies the buoyancy and the location of its inversion corresponds to that of the inversion in temperature. Therefore, the present cases are too simple/specific to be suitable for finding a refinement criterion for the moisture content field. It is argued in the manuscript text that at this early stage within our developments/research, the simplicity of the cases is an advantage.

[2] In this study, the Basilisk 18-02-16 based adaptive grid scheme uses much shorter time-step (between "2 and 15 s" in page 4 line 29) than that of current state of art GCM/SCMs (which is around 10 to 20 minutes and vertical resolution is in the order of at least 100m). Considering Both radiation and vertical diffusion calculation is time consuming, using such a small time step will need much longer computing time. Is it possible to use normal time step of 10-20 minutes for the scheme? If yes, please add new time-step simulation results in Fig.1 to 5; if not, please discuss the limitations of the current adaptive scheme and propose a possible solution;

The reviewer is right to bring forward this 'feature' of the present model. The text mentions that the time integration method is (only) first order accurate (page 4) and this limits the maximum time step of the present model. Also, the fact that the used resolution is much higher than the typical ABL resolution of an operational GCM, the temporal variations in the numerical solution contain contributions of higher frequencies, which warrant a reduced time step. The authors feel that the original manuscript is clear and explicit on the fact that the present model is not an operational GCM. Rather, the the work aims reports on a possible avenue for an adaptive gridding strategy, that is also compatible with higher-order time-integration methods (see e.g. in the work of Rajarshi Roy Chowdhury online: `http://basilisk.fr/sandbox/rajarshi/AllMach_O4/allmach_weno_poisson4_rk4.h`). Therefore, the authors see no reason to expect that the adaptive grid strategy would be incompatible with the time integration strategies as they are currently used in GCM's.

Furthermore, when considering a process such as radiation for which it may be relatively expensive to calculate the corresponding tendency term but that is relatively slow in its evolution. The code also allows to only evaluate these tendencies every so often whilst the grid is able to adapt at intermediate time steps. This is exemplified here: `www.basilisk.fr/sandbox/Antoonvh/smoke.c`, and the results are published in earlier work of the present authors (Van Hooft et al. , 2018).

[3] In Fig. 3, the adaptive grid scheme simulated a slightly unstable (negative) virtual potential temperature profile above 100m while all other models simulate slightly stable (positive) profiles. Is it due to the adaptive-grid scheme or the short-tail stability function used in the model or the Q profile difference,...? It is suggested to also add the fixed- resolution grid scheme results for comparison;

The unstable profile is the results of the used K-closure. All of the other models from the intercomparison use a more recent (read: better) closure for their description of vertical mixing under unstable conditions (see text sect 2.). We have added a notion to this in the results section of the revised manuscript.

We have added a figure below that shows that the slope is controlled by the details of the used closure for turbulent mixing (i.e. the maximum mixing length l, see Sect. 2 of the revised manuscript). Also results for the default mixing length obtained with using the adaptive-grid and equidistant-grid approach are presented. It appears that the difference between both runs is small (max. $0.2K$) and that the slope is virtually identical. We choose not to add there results to the revised manuscript as we feel that it does not add anything new to the present results or would change the analysis.

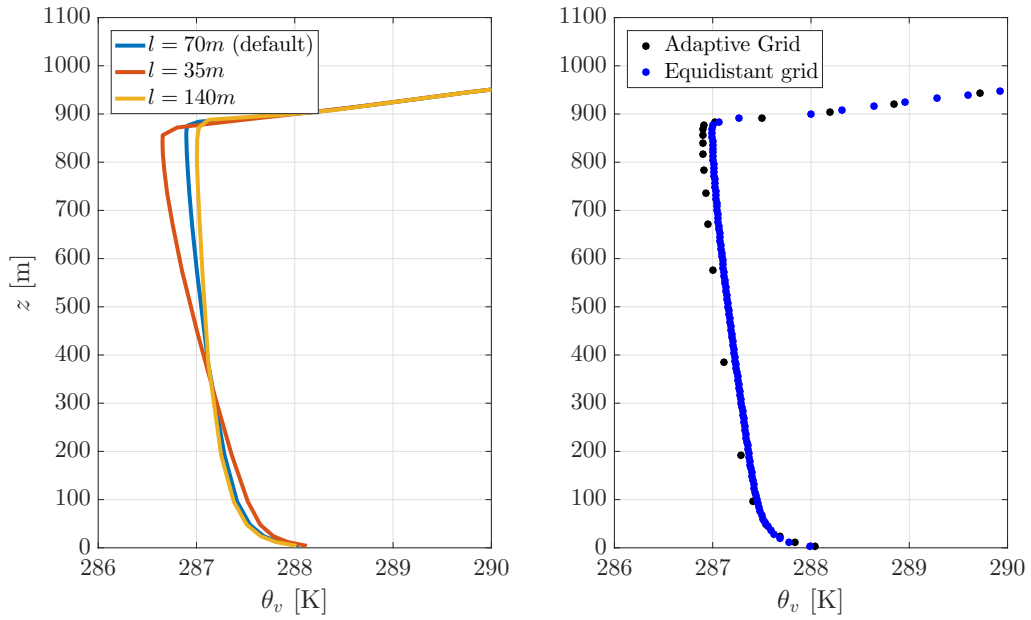

[4] Moist process is important in atmospheric boundary layer variations (both in diurnal and synoptical scale), to exam the effects of adaptive grid scheme on overall PBL simulation, vertical profile comparison of scheme simulated specific humidity Q is suggested to be added in the previous Fig.1;

The reviewer is right that humidity plays an important role in the boundary dynamics. However, the GABLS1 case (corresponding to fig 1) does concern a dry boundary layer, and hence the results for the q profiles are not presented.

[5] Add diurnal cycle of observed and SCM simulated 2m temperature intercomparison (similar like that of Fig.3 c for near surface wind speed) in Fig. 3 in order to better understand the adaptive grid scheme performance

The maximum resolution in this simulation is 8 meters and the temperature at the surface is prescribed by the case definition. Therefore, the suggested statistic is not expected to be very sensitive to the used grid structure, but rather be a test of the used interpolation strategy. Alltough it would be interesting to extend the analysis, in all, the authors are confident that the current set of results supports the message we aim to convey sufficiently.

Response to Reviewer #3

Antoon van Hooft, Stéphane Popinet, and Bas van de Wiel

June 2018

The authors thank the reviewer for taking his/her time to comment on the manuscript. We hope to be able to address all points brought forward by the the reviewer in a point-by-point response in this document accompanied with relevant changes to the manuscript. A PDF highlighting all changes is also provided as a supplement.

The manuscript describes a prototype Single-Column Model (SCM) that employs dynamic grid adaptation in the vertical direction. The adaptations are guided by error estimators which increase the resolution where needed for accuracy, and remove grid points if additional accuracy is not needed. The method is tested in the atmospheric boundary layer based on the two GABLS intercomparison cases. In particular, the GABLS cases test the fine-scale diurnal variations of the planetary boundary layer (PBL). In general, the PBL structures in the two test cases are reasonably well captured in the adaptive SCM. The authors conclude that the adaptive-grid algorithm is able to dynamically coarsen and refine the numerical grid whilst maintaining an accurate solution.
Overall, the manuscript is interesting and well written, but the application area is rather narrow and it is difficult to judge the performance of the model based on two test cases. Therefore, it is difficult to draw more general conclusions concerning 3D General Circulation Models (GCMs). However, this is not the focus of this manuscript, which only addresses a prototype 1D adaptive model. The main criticism is that the description of the adaptive method is rather short which makes it difficult to understand the methodology even at a fundamental level. The main methodology is described in Van Hooft et al. (Boundary-Layer Meteorol., 2018) and the reader is referred to this paper. I recommend expanding the description of the Adaptive Mesh Refinement (AMR) algorithm somewhat in this paper, especially with respect to the error estimation technique. This will help make this a stand-alone paper. In addition, this review lists some clarifying questions that need to be addressed in a revised version.

Leaving out the the details of the error estimation technique was a choice that was made to prevent repetition of material that is published elsewhere. The referenced work in Bound.-Lay. Meteorol. (BLM) can be easily found, is freely available for everyone (open access CC 4.0) and in addition to that the work is also hosted via a mirror website at the HAL repository (`https://hal.archives-ouvertes.fr/hal-01689036`). This provides confidence that an interested reader will be able to find the more detailed information if they wish so. The authors argue that repeating the 3-page story is therefore not necessary and does not really add to the proof-of-principle we aim to illustrate here. In the original manuscript we have opted to briefly describe the algorithm on a more conceptual level. In hindsight we agreee that this may not suffice as it is indeed the key ingredient of the method. Therefore, based on the reviewers suggestion; a serious effort was made to include a didactical example based on an extension of the analysis of the laminar Ekman-spiral case that was formerly in the Appendix (in Sect 3.1). Now the manuscript includes a more detailed analysis of the usage of the error estimation technique. We feel that this is a valuable complementary example of the aforementioned work in the BLM paper, and not a repetition.

Specific comments:
Page 2, line 23: In which way does your work depart from the work by Van Hooft et al. (2018)?

Based on the point brought forward by the reviewer, we realize that we have not chosen our words careful enough here. The new manuscript is revised accordingly.

Page 3, line 17: Define the Richardson number. There are many variants, so please provide the equation.

The revised manuscript is now explicit on the used closures for turbulent transport and states all the relevant definitions.

Page 4, line 12 onwards: Clarifying questions concerning the refinements:
1) Is the grid only refined if both error criteria are fulfilled, or is it enough if one error indicator is flagged?
2) How often do you adapt (e.g. every time step)?
3) How are newly-created grid points initialized, and how are coarsened grid points merged?
4) Is the initialization (interpolation, merging) algorithm mass-conserving with respect to dry air mass & water mass and/or energy conserving?
5) Does the interpolation/merging technique observe the hydrostatic balance? If not, one might expect a lot of gravity waves in 3D versions of this algorithm.
6) Do you interpolate with respect to a height or pressure coordinate in the vertical direction?
7) What is the order of the interpolation technique? If linear, are oscillation-free high-orderinterpolation techniques available?
8) How many ghost cells are used?
9) Typical GCMs work with stretched grids and not equidistant grids. Can your algorithm be applied to stretched grids? The algorithm seems to rely on the fact that the grid spacing differs by exactly a factor of 2 (also refers to Fig. 2).
10) Have other error estimators (variables) and error thresholds been tried? If yes, comment on the pros and cons of these alternative choices.

The following answers in black are added to the main text, the answers in blue are not in the revised manuscript as they are considered off-topic for the present work:
1) If the estimated error in one (or more) of the three (u, v, θ_v) fields exceeds the respective criteria, the corresponding gridcell is refined.
2) The algorithm assesses the fidelity in the representation of the numerical solution at each time step, this garantees that no big developments in the solution take place in between grid adaptations. Noting that, courtesy of the tree-grid data structure, it is computationally cheap to do the assessment and refinement/coarsening compared to doing the time integration (i.e. typically less than 10% of the effort, for the presented cases).
3) For refinement a bilinear interpolation technique is used whose second-order accuracy is consistent with the used solver. For coarsening, two cells can be merged into one by taking their average value which is exact for our finite-volume formulation.
4) The bilinear interpolation technique (for refinement) that is used in this study is not conserving for the first order moments of a scalar field, and not for higher order moments. However, the error introduced by this refinement step is directly controlled by the refinement criteria and can hence be tuned to any desired accuracy. Noting again that the second-order accuracy is inline with the solver's accuracy and hence is consistent with the overall method
5) Yes, see e.g. the 3D studies of van Hooft et al. (2018), or a more clean example online via the link: `http://basilisk.fr/sandbox/Antoonvh/internalwavesAMR.c`
6) No, In the model, height above the surface is used for this purpose instead
7) We use second order accurate bilinear formulation (using a 2-point stencil). Note that a conservative, linear interpolation technique based on a 3-point stencil is available and has an accuracy of the 3-rd order. Recent work of Radjarshi Roy Chowdhury does enable higher-order (of 3-rd, 4-th and 5-th order) methods that are non oscillatory. See an example test of his work that is based on so-called WENO schemes online: `http://basilisk.fr/sandbox/rajarshi/WENO_CODES/weno_prolongation_scaling1D.c`.
8) Two ghost cells are defined foreach resolution boundary and one at each "end" of the domain. This means that that in theory, for a worst-case-scenario, there may be as many ghost-cells as there are "solution grid cells". This is not really a concern since the values of the ghost cells are relatively cheap to calculate and only depend on the values of the "solution grid cells" that are solved for when time integrating the equations (typically $\mathcal{O}(10\%)$). Furthermore, figure 3 shows that the solver is well behaved.
9) The underlying (local) grid structure is Cartesian, and therefore any relevant mapping may be applied/implemented.

(see e.g. `http://basilisk.fr/src/README`). However, the factor of two in the grid resolution between levels of refinement levels is an intrinsic property of the tree-grid structure we use. Our results show that in an ABL the scale separation can differs by two-orders of magnitude within the GABLS2 domain (8m vs 1024m res.), meaning that the factor of two is not really an issue. Alternatively, adaptive unstructured grids exist that do not have this limitation (e.g. the code by the name of "fluidity" `http://fluidityproject.github.io/`). However, a complete discussion of the pro's and con's of such an approach would entail a new study of its own and is a considered to be outside the scope of the present work. Finally, the reference work of Dunbar (2008) uses dynamical grid stretching. But the authors would not call such a dynamic approach to be truly adaptive (see text).

10) Yes, this was part of the tria l-and-error approach and the pro's and con's may be obvious from the analysis in the new Sect. 3.1. The values of the refinement criteria may be used to tune the balance between accuracy and the speed performance of the code. Furthermore, for cases that are more driven by e.g. cloud-top radiation etc. it would be sensible to also refine based on the estimated errors in the moisture fields and cloud fraction field. Similar to pre-tuning a static grid, the balance between accuracy and speed performance remains at the discretion of the model user. The authors feel that the adaptation algorithm provides a more user-friendly, consistent and mathematically-rigorous approach compared to pre-tuning a stretched grid. This is especially true when the results from a model run are not know beforehand. Yet we cannot provide a universal recipe for finding suitable refinement-criterion values and this is part of our continued research.

Page 4, Eqs. (4)-(6): Since all operators are 1D, I suggest using partial derivatives with respect to z instead of the Laplacian operator in Eqs. (4) – (6)

The equations are updated according to the reviewers suggestion

Page 4, line 29: The time steps are extremely short. Can the adaptive method also be applied to more usual physics time steps on the order of minutes to half an hour?

The time-integration scheme is only first-order accurate and this hampers the time stepping. Not the adaptive grid scheme as we see a similar deterioration in our results for the fixed-grid solution when the time stepping parameter is relaxed to larger values. Additionally, time stepping is small because the fine-scale features that are resolved, courtesy of the $O(10m)$ resolution. We note that there would be no reason to assume that adaptive-grids and/or the Basilisk code cannot handle the style of time-stepping schemes of operational GCM's. We argue that the manuscript is clear on the fact that we do not aim to present a GCM but we rather focus on a possible avenue for it's gridding.

Page 5, line 10: the geostrophic flow cannot be described as a 'forcing' mechanism. A forcing term needs units of m/s^2 .

The reviewer is right, the text has been improved accordingly in the revised manuscript.

Page 5, line 19: is this the potential temperature or virtual potential temperature? Fig. 1 shows the potential temperature, Fig. 3 show the virtual potential temperature. Is this difference intentional (provide some reasoning)?

We simply follow the original intercomparison papers regarding GABLS1 and GABLS2 of Cuxart et al. (2006) and Svensson et al. (2011), respectively. We think their reasoning was that the GABLS1 case is dry and hence the concept of virtual potential temperature is not relevant over the its non-virtual counterpart. This is not thecase for GABLS2, where in the original work of Svensson et al. it was chosen to intercompare the virtual potential temperature.

Page 5, line 17: should read 'physical closures for K'
Page 5, line 23: should read 'turbulent transport coefficient'
Page 5, line 28: should read 'on the order'
Page 6, Fig. 3: explain the meaning of the gray shading
Page 6, line 22: should read 'Fig. 5'
Page 6, line 27, should read 'presented a one-dimensional'
Page 7, line 15: explain acronym RANS
Page 8, Appendix: what is the equation that is solved here?
Page 8, line 10: provide the values for gamma, U geo , the Coriolis parameter f, and the density rho
Page 8, line 19: Start sentence with 'The adaptive' instead of 'Were'.
Page 10, line 32: Update the Van Hooft et al. reference
Page 14, Table 1: State 'Number of time steps' instead of 'Solver timesteps'
Page 14, caption of Fig. A1: explain that the slope of the dashed line shows the second-order accuracy

We thank the reviewer again for his/her carefull reading of the manuscript and hope to have adressed all these points at their corresponding locations in the revised manuscript.
Except that we have not added the numerical values for U_{geo}, Ω etc... In stead, based on the reviewers comment, we present the results now in a properly scaled frame work. Making the results universal, as is allowed by the fact that the (scaled) analytical Ekman solution is not a function of the dimensionless ratio: $\Pi = \frac{U_{geo}\gamma}{\nu}$.

Adaptive Cartesian Meshes for Atmospheric Single-Column Models, a study using Basilisk 18-02-16

J.Antoon van Hooft[1], Stéphane Popinet[2], and Bas J.H. van de Wiel[1]

[1]Delft University of Technology, Department of Geoscience and Remote Sensing, Delft, The Netherlands
[2]Sorbonne Université, Centre National de Recherche Scientifique, UMR 7190, Institut Jean Le Rond D'Alembert, F-75005, Paris, France

Correspondence to: Antoon van Hooft (j.a.vanhooft@tudelft.nl)

Abstract. It is well known that the representation of certain atmospheric conditions in climate and weather models can still suffer from the limited grid resolution that is facilitated by modern-day computer systems. Herein we study a simple one-dimensional analogy to those models by using a Single-Column Model (SCM) description of the atmosphere. The model employs an adaptive Cartesian mesh that applies a high-resolution mesh only when and where it is required. The so-called adaptive-grid model is described and we report on our findings obtained for tests to evaluate the representation of the atmospheric boundary layer, based on the first two GABLS intercomparison cases. The analysis shows that the adaptive-grid algorithm is indeed able to dynamically coarsen and refine the numerical grid whilst maintaining an accurate solution. This is an interesting result as in reality, transitional dynamics (e.g. due to the diurnal cycle or due to changing synoptic conditions) are rule rather than exception.

1 Introduction

Single-Column Models (SCMs) are often used as the building blocks for Global (or General) Circulation Models (GCMs). As such, many of the lessons learned from SCM development can be inherited by GCMs and hence the evaluations of SCMs ~~receives~~ receive considerable attention by the geoscientific model development community (see e.g. Neggers et al., 2012; Bosveld et al., 2014; Baas et al., 2017). In this work, we present a SCM that employs an adaptive Cartesian mesh that can drastically reduce the computational costs of such models, especially when pushing the model's resolution. The philosophy is inspired by recently obtained results on the evolution of atmospheric turbulence in a daytime boundary layer using ~~three dimensional~~ three-dimensional (3D) adaptive grids. As promising results were obtained for ~~turbulence resolving~~ turbulence-resolving techniques such as Direct Numerical Simulations and Large-eddy Simulation (LES), herein we explore whether similar advancements can be made with more practically oriented techniques for the numerical modelling of the atmosphere. As such, the present model uses Reynolds-averaged Navier-Stokes ~~techniques (Reynolds, 1895) to parameterize~~

(RANS) techniques to parametrize the vertical mixing processes due to turbulence (Reynolds, 1895), as is typical in weather and climate models.

The discussion of limited grid resolution is present in many studies of SCMs and GCMs. A prominent example is the nocturnal cumulus-cloud case (Wyant et al., 2007): whereas a high resolution mesh is required for capturing the processes at the cloud interface, a coarser resolution may be used for the time when the sun has risen and the cloud has been dissolved. More generally speaking, virtually all of the atmospheric dynamics that require a relatively high-resolution grid for their representation in numerical models are localized in both space and in time. The issue is made more difficult to tackle by the fact that their spatio-temporal localization is typically not known a priori (e.g. the height and strength of a future inversion layer). Therefore, the pre-tuned and static-type grids that most operational GCMs use (virtually all) are not flexible enough to capture all dynamical regimes accurately or efficiently. This also puts a large strain on the used closures for the sub-grid scale processes. In order to mitigate this challenge, GCMs that employ a so-called adaptive grid have been explored in the literature. Here the grid resolution adaptively varies in both space and time, focussing the computational resources to where and when they are most necessary. Most notably, the innovative works of Jablonowski (2004), Jablonowski et al. (2009) and St-Cyr et al. (2008) report on the usage of both Cartesian and non-conforming three-dimensional adaptive grids and clearly demonstrate the potential of grid adaptivity for GCMs. Inspired by their works, we follow a 1D SCM approach and aim to add to their findings, using different grid-adaptative formulations and solver strategies. Since SCMs do not resolve large-scale atmospheric circulations, the analysis herein focusses on the representation of the Atmospheric Boundary Layer (ABL).

Over the years, the computational resources that are available to run computer models have increased considerably (Schaller, 1997). This has facilitated GCMs to increase their models' spatial resolution, enabling to better resolve the most demanding processes. However, it is important to realize that ~~for virtually all physical processes,~~ the (spatial and temporal) fraction of the domain that ~~actually calls for the~~ benefits most from an increasing maximum resolution ~~decreases~~necessarily decreases as separation of the modelled spatial scales increases (Popinet, 2011). This is because the physical processes that warrant a higher-resolution mesh are virtually never space filling. E.g. the formation phase of tropical cyclones is localized in both space and time and is characterized by internal dynamics that evolve during the formation process. By definition, with an increasing ~~resolved~~ scale separation, only an adaptive-grid approach is able to reflect the effective (or so-called fractal) dimension of the physical system in the scaling of the computational costs (Popinet, 2011; Van Hooft et al., 2018). This is an ~~important~~ aspect where the present adaptive-grid approach differs from for example, a dynamic-grid approach (see e.g. Dunbar et al., 2008), that employs a fixed number of grid cells that needs to be predefined by the user. This work ~~departs from the~~ employs a similar method for grid adaptation as presented in the work of Van Hooft et al. (2018) on 3D-turbulence-resolving simulations of the ABL. As such, this work is also based on the adaptive-grid toolbox and build-in solvers provided by the 'Basilisk' code (http://basilisk.fr).

We test our model with the well established cases defined for the first two GABLS intercomparison projects for SCMs. As part of the Global Energy and Water cycle EXchanges (GEWEX) modelling and prediction panel, the GEWEX ABL Study (GABLS) was initiated in 2001 to improve understanding of the atmospheric boundary layer processes and their representation in models. Based on observations during field campaigns, a variety of model cases has been designed and studied using

both LES and SCMs with a large set of models using traditional static-grid structures. An overview of the results and their interpretation for the first three intercomparison cases are presented in the work of Holtslag et al. (2013). Here we will test the present adaptive-grid SCM based on the first two intercomparison cases, referred to as GABLS1 and GABLS2. These cases were designed to study the model representation of the stable boundary layer and the diurnal cycle, respectively. Their scenarios prescribe idealized atmospheric conditions and lack the complete set of physical processes and interactions encountered in reality. At this stage within our research, the authors consider this aspect to be an advantage, as the present SCM model does not have a complete set of parametrizations for all processes that are typically found in the operational models (see e.g. Slingo, 1987; Grell et al., 2005)).

This paper is organized as follows, the present SCM is discussed in more detail in Sect. 2. ~~The results~~ Based on the results from a simplified flow problem, Sect. 3 starts with an analysis of the used numerical methods and the grid adaptation strategy. Model results for ABL-focussed cases that are based on the first two GABLS intercomparison scenarios are also presented in Sect. 3. Finally, a discussion and conclusions are presented in Sect. 4. ~~Furthermore, in the Appendix ??, a validation of the used solver formulation is given for a simplified flow problem (i.e. the laminar Ekman spiral).~~

2 Model Overview

As we focus on the merits of grid adaptivity in this study on SCMs and not on the state-of-the-art closures for the vertical transport phenomena, we have opted to employ simple and well-known descriptions for the turbulent transport processes. More specifically, the present model uses a stability-dependent, first-order, local, K-diffusivity closure as presented in the seminal works of Louis (1982) and Beljaars et al. (1989). For the surface-flux parametrizations we again follow the work of Louis (1982). ~~The used closures are not repeated here but are summarized in section 2 of Holtslag and Boville (1993).~~ However, to improve the representation of mixing under stable conditions, an alteration is made to the formulation of the so-called stability-correction function ~~(F(Ri))~~ under stably-stratified conditions. Based on the work of England and McNider (1995), we use a so-called short-tail mixing function~~,~~. The used closures for the turbulent transport are summarized next. The *surface* fluxes (F) of the horizontal velocity components (u, v), the potential temperature (θ) and specific humidity q are evaluated as:

$$F(\mathrm{Ri})_u = C_M U_1 u_1, \tag{1a}$$

~~where Ri is the local and~~

$$F_v = C_M U_1 v_1, \tag{1b}$$

$$F_\theta = C_H U_1 (\theta_1 - \theta_0), \tag{1c}$$

$$F_q = C_H U_1 (q_1 - q_0), \tag{1d}$$

Where U is the wind-speed magnitude and indices 0 and 1 refer the to values at the surface and the first model level, respectively. The surface transport coefficients are,

$$C_M = C_N f_{s,M}(\mathrm{Ri_b}), \tag{2a}$$

$$C_H = C_N f_{s,H}(\mathrm{Ri_b}), \tag{2b}$$

with $\mathrm{Ri_b}$ the surface bulk Richardson number~~for the evaluation of turbulent diffusivities and~~, that is defined as,

$$\mathrm{Ri_b} = \frac{g}{\theta_{v,\mathrm{ref}}} \frac{z_1 \left(\theta_{v,0} - \theta_{v,1}\right)}{U_1^2}, \tag{3}$$

where g is the acceleration due to gravity, θ_v is the virtual potential temperature and $\theta_{v,\mathrm{ref}}$ a corresponding reference value. The so-called neutral exchange coefficient (C_N) is calculated using,

$$C_N = \frac{k^2}{\ln\left((z_1 + z_{0,M})/z_{0,M}\right)^2}, \tag{4}$$

with $k = 0.4$ the Von Karman constant, z_1 the height of lowest model level and $z_{0,M}$ is the roughness length for momentum. For the cases studied in this work, the roughness length for heat is assumed to be identical to $Z_{0,M}$. The stability correction functions for the surface transport ~~, respectively. The~~ of momentum and heat ($f_{s,M}, f_{s,H}$) are,

$$f_{s,M}(\mathrm{Ri_b}) = \begin{cases} 0, & \mathrm{Ri_b} \geq 0.2, \\ \left(1 - \frac{\mathrm{Ri_b}}{0.2}\right)^2, & 0 \leq \mathrm{Ri_b} < 0.2, \\ 1 - \frac{10\mathrm{Ri_b}}{1+75C_N\sqrt{((z_1+z_{0,M})/z_{0,M})\|\mathrm{Ri_b}\|}}, & \mathrm{Ri_b} < 0, \end{cases} \tag{5a}$$

$$f_{s,H}(\mathrm{Ri_b}) = \begin{cases} f_{s,M}(\mathrm{Ri_b}), & \mathrm{Ri_b} \geq 0, \\ 1 - \frac{15\mathrm{Ri_b}}{1+75C_N\sqrt{((z_1+z_{0,M})/z_{0,M})\|\mathrm{Ri_b}\|}}, & \mathrm{Ri_b} < 0, \end{cases} \tag{5b}$$

which conclude the discription of the surface fluxes. The vertical flux ($\overline{w'a'}$) of a dummy variable a due to turbulence within the boundary layer is based on a local diffusion scheme and is expressed as,

$$\overline{w'a'} = -K\frac{\mathrm{d}a}{\mathrm{d}z}, \tag{6}$$

where K is the so-called eddy diffusivity,

$$K = l^2 S f(\mathrm{Ri}). \tag{7}$$

l represents an effective mixing length,

$$l = \min\left(kz, l_{bl}\right), \tag{8}$$

with l_{bl} is the Blackadar length scale, we use, $l_{bl} = 70m$ (Holtslag and Boville, 1993). S is the local wind-shear magnitude,

$$S = \|\frac{\mathrm{d}U}{\mathrm{d}z}\|, \tag{9}$$

and $f(\mathrm{Ri})$ is the stability correction function for the vertical flux,

$$f(\mathrm{Ri}) = \begin{cases} 0, & \mathrm{Ri} \geq 0.2, \\ \left(1 - \frac{\mathrm{Ri}}{0.2}\right)^2, & 0 \leq \mathrm{Ri} < 0.2, \\ \sqrt{1 - 18\mathrm{Ri}}, & \mathrm{Ri} < 0, \end{cases} \tag{10}$$

i.e. based on the gradient Richardson number,

$$\mathrm{Ri} = \frac{g}{\theta_{v,ref}} \frac{\mathrm{d}\theta_v/\mathrm{d}z}{S^2}. \tag{11}$$

The authors of this work realize that there ~~has~~ have been considerable advancements on the representation of mixing under unstable conditions in the past decades, e.g non-local mixing (Holtslag and Boville, 1993) and turbulent-kinetic-energy-based closures (see e.g., Mellor and Yamada, 1982; Lenderink and Holtslag, 2004). Therefore, we would like to note that such schemes are compatible with the adaptive-grid approach and they could be readily employed to improve the physical descriptions in the present model. From an implementations' perspective, those schemes would not require any grid-adaptation specific considerations when using the Basilisk code.

The most prominent feature of the SCM presented in this work is its ability to dynamically coarsen and refine the grid resolution based on the evolution of the solution itself. As mentioned in the introduction, the associated grid-adaptation algorithm is the same as was used by Van Hooft et al. (2018). We only briefly discuss the general concept here. For an in-depth quantitative discussion with ~~an example~~simplified examples, the reader is referred to the aforementioned paper.

Apart from the imperfect representation of the physical aspects of a system in numerical models, additional errors naturally arise due to the spatial and temporal discretization. In general, a ~~higher~~ finer resolution corresponds to a more accurate solution and a simulation result is considered to be 'converged' when the numerically obtained solution and its statistics of interest do not crucially depend on the chosen resolution. The aim of the grid-adaptation algorithm is to dynamically coarsen and refine the mesh so that the errors due to the spatial discretization remain within limited bounds and to be *uniformly distributed* in both space and time. For our adaptive approach this requires, (1) an algorithm that evaluates a local estimate of the discretization error in the representation of selected solution fields (χ_a for a field 'a') and (2), a corresponding error threshold ($\xi\zeta_a$) that determines if a grid cell's resolution is either too ~~fine, too coarse~~ coarse (i.e. $\chi_a > \zeta_a$), too fine (i.e. $\chi_a < 2\zeta_a/3$), or just fine.

Grid adaptation can then be carried out accordingly and the solution values of new grid cells can be found using interpolation techniques. A cell is refined when the estimated error for at least one selected solution field exceeds it's refinement criterion and a cell is coarsened when it is considered to be 'too fine' for all selected solution fields. The 'error estimator' (χ) is based on a so-called multi-resolution analysis that is formally linked to wavelet thresholding. The algorithm aims to estimate the magnitude of higher-order contributions in the spatial variability of the solution that are not captured by the solver's numerical schemes. Consistent with the second-order spatial accuracy of the solver's numerical schemes (Popinet, 2017b), the algorithm employs a second-order accurate wavelet-based error estimate. In practice, grid refinement will typically occur at the locations where the solution is highly 'curved', whereas those areas where the solution fields vary more 'linearly' in space are prone to coarsening. The error threshold, or so-called refinement criterion ζ, is defined by the user. Noting that similar to the pre-tuning of the fixed-in-time grids as is common in most SCMs, the ~~grid resolution~~ balance between accuracy and the required computational effort remains at the discretion of the model's user.

~~In this work~~ For the cases in this work that focus on the ABL (i.e. in Sect 3.2 and 3.3), the dynamics are governed by the wind ($\boldsymbol{U} = (u, v)$) and the virtual potential temperature (θ_v), hence we base the refinement and coarsening of the grid on a second-order-accurate estimated ~~discretization error in the solution fieldsfor the horizontal wind components ($\boldsymbol{u} = (u, v)$) and the virtual potential temperature (θ_v)~~error associated with the represenation of these discretized fields. Based on ~~trail~~ trial and error, we set the corresponding refinement ~~criteria~~thresholds,

$$\zeta_{u,v} = 0.25 \text{ m/s}, \tag{12}$$

$$\zeta_{\theta_v} = 0.5 \text{ K}, \tag{13}$$

for both of the horizontal wind components and virtual potential temperature, respectively. ~~In practice, the grid-adaptation algorithm strongly relates the resolved local 'curvature'~~ These values are the result of an choice by the authors that aims to strike an arbitrary balance between the accuracy of the solution ~~fields to the local grid resolution, where high curvature corresponds to a high resolution~~and the computational effort required to run the model. Note that a similar (arbitrary) balance needs also to be found when static grids are employed. For a simple flow set-up, Sect. 3.1 presents an example convergence study to show the effects of using different refinement criteria on the obtained solutions.

Grid adaptation is carried out each time step. The tree-based anisotropic-grid structure in Basilisk facilitates a convenient basis for the multi-resolution analysis and the subsequent refinement and coarsening of cells at integer levels of refinement. This entails that the spatial resolution can vary by factors of two (Popinet, 2011). For the adaptive-grid runs presented in this paper, the time spend in the actual grid assessment and adaptation routines is less than than 5% of the total wall-clock time (see table 1).

For time integration; we recognize a reaction-diffusion-type equation describing the evolution of the horizontal wind components and scalar fields such as the virtual potential temperature and specific humidity (q_t). For a variable field $s(z,t)$, we write,

$$\frac{\partial s}{\partial t} = \nabla \frac{\partial}{\partial z} \cdot (K \nabla \frac{\partial}{\partial z} s) + r. \tag{14}$$

Where r is a source term and K is the diffusion coefficient. Using a time-implicit first-order-accurate time discretization with ~~timestep~~ time step Δt separating the solution s^n and s^{n+1}, this can be written,

$$\frac{s^{n+1}-s^n}{\Delta t} = \nabla \frac{\partial}{\partial z} \cdot (K \nabla \frac{\partial}{\partial z} s^{n+1}) + r. \tag{15}$$

Rearranging the terms we get,

$$\nabla \frac{\partial}{\partial z} \cdot (K \nabla \frac{\partial}{\partial z} s^{n+1}) - \frac{s^{n+1}}{\Delta t} = -\frac{s^n}{\Delta t} - r. \tag{16}$$

To obtain a Poisson-Helmholtz equation~~, that is solved for~~. Eq. 16 is solved using a multigrid strategy, employing a finite-volume-type second-order-accurate spatial discretization (Popinet, 2017a, b). ~~The physical timestep~~ Apart from the Ekman-spiral case in Sect. 3.1, the physical time step in the ABL-focussed cases is adaptively varied between 2 sec. and 15 sec. based on the convergence properties of the aforementioned iterative solver. Noting that these values are rather small compared to existing SCMs that often employ higher-order-accurate time-integration schemes. Aditionally, the correlation of spatial and temporal scales warrants a smaller time step, since the present model employs a higher maximum vertical resolution compared to that of an operational GCM. The solver's second-order spatial accuracy is validated and its performance scaling is accessed for a simple flow set-up in ~~Appendix ??~~Sect. 3.1. For the exact details of the model set-ups for the cases presented in this paper, the reader is referred to the case-definition files (in legible formatting). Links are provided to their online locations in table 1.

3 Results

3.1 The Ekman spiral and grid adaptation

Before we focus our attention on cases that concern the ABL, this section discusses the philosophy of the used grid adaptation strategy based on the analysis of a one-dimensional (1D) Ekman-flow set-up. This simple and clean set-up enables to quantify numerical errors explicitly and test the solver's numerical schemes. The aim of this section is to show that the grid-adaptation strategy and the accompanying refinement criteria provide a consistent and powerful framework for adaptive mesh-element-size selection. Results are presented for both an equidistant-grid and the adaptive-grid approach. The case describes a neutrally-stratified fluid with kinematic viscosity ν and density ρ in a rotating frame of reference with angular velocity Ω. A flow is forced by a horizontal pressure gradient $\mathrm{d}P/\mathrm{d}y = U_{geo} f \rho$, over a no-slip bottom boundary (located at $z_{bottom} = 0$). Where U_{geo} is a velocity scale that is also known as the geostrophic wind. There exists an analytical, 1D, steady solution for the horizontal wind components (u_E, v_E), that is known as the Ekman spiral;

$$u_E = U_{geo}\left(1 - e^{-\gamma z}\cos(\gamma z)\right), \tag{17}$$

$$v_E = U_{geo} e^{-\gamma z}\sin(\gamma z), \tag{18}$$

with γ the so-called Ekman depth, $\gamma = \sqrt{\Omega/\nu}$. We initialize the solution according to the exact solution and set boundary conditions based on Eqs. 17 and 18. Equation 14 is solved numerically for both u and v components without any closures for

turbulent transport, on a domain with height $z_{top} = 100\gamma$. The simulation is run until $t_{end} = 10 \times \gamma/U_{geo}$, using a small time step $\mathrm{d}t = 0.01 \times \gamma/U_{geo}$. The time step is chosen such that the numerical errors are dominated by the spatial discretization rather than by the time-integration scheme. During the simulation run, discretization errors alter the numerical solution from it's exact, and analytically steady, initialization. For all runs, the diagnosed statistics regarding the numerical solutions that are presented in this section have become steady at $t = t_{end}$.

The spatial-convergence properties for the equidistant-grid solver are studied by iteratively decreasing the used (equidistant) mesh-element sizes (Δ) by factors of two and we monitor the increasing fidelity of the solution at $t = t_{end}$ between the runs. Therefore, based on the analytical solution, a local error ($\epsilon_{u,v}$) of the numerically obtained solution (u^n, v^n) within each grid cell is diagnosed and is defined here as:

$$\epsilon_a = \| a^n - \langle a_E \rangle \|, \tag{19}$$

where a is a dummy variable for u and v, $\langle a_E \rangle$ is the grid-cell-averaged value of the analytical solution (a_E) and a^n the value of the numerical solution within the cell[1]. Figure 1a shows the results and compares the used grid resolution (Δ) with the error $\epsilon_{u,v}$. It appears that the observed range of ϵ-values is large and typically spans 10 orders of magnitude, with a lower bound defined by the 'machine precision' (i.e. $\approx 10^{-15}$ for double-precision floating-point numbers). This wide range can be explained by the fact that the Ekman spiral is characterized by exponentially decreasing variation with height (see Eqs. 17, 18) and hence the equidistant grid may be considered overly refined at large z. This illustrates that, for a given solver formulation, the error in the solution is not directly dictated by the mesh-element size, but also depends on *the local shape of the numerical solution itself*. This poses a challenge for the pre-tuning of meshes applied to GCMs, where a balance need to be found between accuracy and computational efficiency. The solution of a future model run is not known beforehand and hence the tuning of the grid typically relies heavily on experience, empericism and a-priori knowledge. This motivates to apply the method of error *estimation* in the representation of a discretized solution field as described in Popinet (2011) and Van Hooft et al. (2018). For both velocity components, this estimated error ($\chi_{u,v}$) is evaluated at the end of each simulation run for each grid cell and is plotted against the corresponding error ($\epsilon_{u,v}$) in Fig. 1b. It seems that for this virtually steady case, there is a clear correlation between the diagnosed (instantaneous) χ-values and the ϵ-values that have accumulated over the simulation run time. Even tough the correlation is not perfect, it provides a convenient and consistent framework for a grid adaptation algorithm. As such, a second convergence test for this case is performed using a variable-resolution grid within the domain. The mesh is based on the aforementioned adaptive-grid approach. For these runs, we iteratively decrease the so-called refinement criterion ($\zeta_{u,v}$) by factors of two between the runs and monitor the increasing fidelity of the numerically obtained solution for all runs. The refinement criterion presets a threshold value (ζ) for the estimated error χ that defines when a cell should be refined ($\chi > \zeta$) or alternatively, when it may be coarsened ($\chi < 2\zeta/3$). Figure 2a presents the results and compares the used local grid resolution against $\epsilon_{u,v}$ for the various (colour-coded) runs. It appears that for all separate runs, the algorithm employed a variable resolution mesh and that this has resulted in a smaller range of the local error in the solution (ϵ). The local error in the solution is also compared against the wavelet-based estimated error in the representation of the solution fields in Fig.

[1] a^n (also) represents the grid-cell-averaged value in a finite-volume approach.

2b. Compared to the results from the equidistant-grid approach as presented in Fig. 1b), the spread of the χ and ϵ values is relatively small for the separate runs when the adaptive-grid approach is used. The most prominent reason for the finite spread is that the error (ϵ) was diagnosed after 1000 time steps. This facilitated errors in the solution that arise at a specific location (with a large χ-value) to 'diffuse' over time towards regions where the solution remains to be characterized by a small χ-value (not shown). Also, since u and v are coupled (due to the background rotation), local errors that arise in solution for u 'pollute' the v-component solution, and vice versa. Furthermore, a spread is expected because the tree-grid structure only allows the resolution to vary by factors of two (Popinet, 2011).

Finally, the global convergence characteristics and the speed performance of the two approaches are studied. The global error (η) in the numerically obtained solution is evaluated as,

$$\eta = \int_{z_{bottom}}^{z_{top}} (\epsilon_u + \epsilon_v)\,\mathrm{d}z, \tag{20}$$

In order to facilitate a comparison between the methods, we diagnose the number of used grid cells (N) for the adaptive-grid run. Figure 3a shows that for both approaches the error scales inversely proportional to the used number of grid cells to the second power (i.e. second-order spatial accuracy in 1D). The adaptive grid results are more accurate than the results from the fixed-grid approach when employing the same number of grid cells. Figure 3b shows that for both approaches the required effort (i.e. measured here in wall-clock time) scales linearly with the number of grid cells, except for the runs that require less than one-tenth of a second to perform. The plots reveals that *per grid cell* there is computational overhead for the adaptive-grid approach. These results show that the used numerical solver is well behaved.

The following sections are devoted to testing the adaptive-grid approach in a more applied SCM scenario, where the turbulent transport closures are applied (see Sect. 2) and the set-up is unsteady. Here, the quality of the adaptive-grid solution has to be assessed by comparing against reference results from other SCMs, large-eddy simulations and the present model running in equidistant-grid mode.

3.2 GABLS1

The first GABLS intercomparison case focusses on the representation of a stable boundary layer. Its scenario was inspired by the LES study of an ABL over the Arctic sea by Kosović and Curry (2000). The results from the participating SCMs are summarized and discussed in Cuxart et al. (2006), for the LES intercomparison study, the reader is referred to the work of Beare et al. (2006). The case prescribes the initial profiles for wind and temperature, a constant ~~geostrophic forcing~~ forcing for momentum corresponding to a geostrophic wind of $U_{geo} = 8$ m/s and a fixed surface-cooling rate of 0.25 K/hour. The model is set-up accordingly, with a maximum resolution of 6.25 meter ~~, corresponding to 6 levels of refinement~~ and a domain height of 400 meters. The maximum resolution corresponds to 6 levels of tree-grid refinement, where each possible coarser level corresponds to a factor of two increase in grid size.

Due to the idealizations in the case set-up with respect to the reality of the field observations, the model results were not compared against the experimental data (Cuxart et al., 2006). However, for the SCMs, a reference was found in the high-

fidelity LES results that tended to agree well between the various models. The LES results therefore serve as a benchmark for the results obtained with the present model. This facilitates a straight forward testing of the formulations and implementations of the used physical closures, before we continue our analysis towards the full diurnal cycle. Inspired by the analysis of Cuxart et al. (2006) and *their* figure 3, we compare our SCM results with the 6.25 meter-resolution LES ensemble results. We focus on the profiles for the wind components and potential temperature averaged over the eighth hour of the simulation in Fig. 4. We observe that the present SCM is in good agreement with the LES results and is able to capture the vertical structure of the ABL, including the low-level jet. The differences are only minor compared to the variations in the results presented in the aforementioned GABLS1 SCM reference paper.

~~Noting~~ Note that in general, results are of course sensitive to the closure chosen to parametrize the turbulent transport, in our case given by ~~Eq.5~~ Eqs.5 and 10. In order to separate between the numerical effects of using grid adaptivity and the chosen physical closures, we define an additional reference case in which we run an *equidistant-grid* SCM. This model run employs a fixed 6.25 meter resolution (i.e with 64 cells), but otherwise identical closures and numerical formulations. I.e. we have switched-off the grid adaptivity and maintain the maximum resolution throughout the domain. We can observe that results between both SCMs are in good agreement but, that minor deviations are present. These discrepancies are in the order of magnitude of the refinement criteria and can be reduced by choosing more stringent values~~(see Appendix ??)~~, that would result in using more grid cells. The evolution of the adaptive-grid structure is shown in Fig. 5 a. We see that a relatively high resolution is employed near the surface, i.e. in the logarithmic layer. Remarkably, without any a priori knowledge, the grid is refined at a height of $150\ \mathrm{m} < z < 200\ \mathrm{m}$ as the so-called low-level jet develops, whereas the grid has remained coarse above the boundary layer where the grid resolution was reduced to be as coarse as 100 meters. From Fig.5 b we learn that the number of grid cells varied between 11 and 22 over the course of the simulation run.

3.3 GABLS2

The second GABLS model intercomparison case was designed to study the model representation of the ABL over the course of two consecutive diurnal cycles. The case is set-up after the observations that were collected on the ~~22th and~~ 23rd and 24th of October, 1999 during the CASES-99 field experiment in Leon, Kansas, USA (Poulos et al., 2002). The ~~details are described (and not repeated here)~~ case prescribes idealized forcings for two consecutive days that were characterized by a strong diurnal cycle pattern. During these days, the ABL was relatively dry and there were few clouds. The details of the case are described in the work of Svensson et al. (2011) that was dedicated to the evaluation of the SCM results for the GABLS2 intercomparison. Compared to the original case prescriptions, we choose a slightly higher domain size of $z_{top} = 4096$ meters (compared to 4000 m), so that a maximum resolution of 8 meters corresponds to 9 levels of refinement.

In this section we place our model output in the context of the results presented in the work of Svensson et al. (2011), that, apart from the SCM results, also includes the results from the LES by Kumar et al. (2010). To obtain their data we have used the so-called 'data digitizer' of Rohatgi (2018). Inspired by the analysis of Svensson et al. (2011) and *their* figures 10 and 11, we intercompare our results for the wind-speed magnitude ($U = \|\boldsymbol{u}\|$) and virtual potential temperature profiles in Fig. 6 a and b, respectively. Here we see that the results obtained with the present SCM fall within the range of the results as were

found with the selected models that participated in the original intercomparison. These models also employed a first-order-style turbulence closure and have a lowest model-level height of less than 5 meters. ~~Fig.~~ The present modelled virtual potential temperature (θ_v) shows a slight negative vertical gradient in the well mixed layer. This is a feature related to the usage of the local K-diffusion description for the turbulent transport (see Sect. 2 and the work of Holtslag and Boville (1993)). Figure 6 c presents a timeseries of the 10-meter wind speed (U_{10m}) during the ~~22-th~~ 23-rd of October. Again the present model results compare well with the others. Next, in order to validate the grid-adaptivity independently from the used closures, we present the hourly evolution of the wind speed on the ~~23-rd~~ 24-th of October against the results obtained with adaptivity switched off, using 512 *equally-spaced* grid points in Fig. 7. ~~We clearly see that the~~ A nearly identical evolution of the wind speed ~~profile is the same~~ profiles is observed and even the small-scale features in the inversion layer (i.e. $z \approx 800$ m) are present in the ~~adaptive-grid model~~ adaptive-grid-model calculations. The corresponding evolution of the adaptive-grid structure is presented in Fig. 5, where the colours in the resolution plot appear to sketch a 'Stullian' image, showing a prototypical diurnal evolution of the ABL (see figure 1.7 in the book of Stull, 1988). Apparently, the grid-adaptation algorithm has identified (!) the 'surface layer' within the convective boundary layer, the stable boundary layer, the entrainment zone and the inversion layer as the dynamic regions that require a high-resolution mesh. Conversely, the well-mixed layer within the CBL, the residual layer and the free-troposphere are evaluated on a coarser mesh. The total number of grid cells varied between 24 and 44.

4 Discussion & Conclusions

In this work we have presented an one-dimensional (1D) single-column model (SCM) that employs a mesh whose resolution is varied adaptively based on the evolution of the numerically obtained solution. This is an attractive feature because it is a prerequisite to enable the computational effort required for the evaluation of numerical solution to scale with the complexity of the studied physical system. The adaptation algorithm based on limiting discretization errors appears to function very well for a wide variety of geophysical applications: e.g. 3D atmospheric turbulence-resolving models (Van Hooft et al., 2018), tsunami and ocean-wave modelling (Popinet, 2011; Beetham et al., 2016; Marivela-Colmenarejo, 2017), hydrology (Kirstetter et al., 2016), two-phase micro physics (Howland et al., 2016), flow of granular media (Zhou et al., 2017) and shock-wave formation (Eggers et al., 2017). For these studies on highly dynamical systems, the adaptive-grid approach is chosen because it offers a more computationally ~~effcient~~ efficient approach as compared to the usage of static grids.

The present work does not include an in-depth assessment and discussion on the performance of the presented methods in relation to the computational speed. Even though this is an important motivation for the application of the adaptive-grid strategy to GCMs, the authors argue that an SCM is not suitable for speed-performance testing: the speed of single-column calculations is virtually never a critical issue. Only in 3D mode, when SCMs are 'stitched together' to enable the resolving of global circulations, the model's computational efficiency becomes an issue. Furthermore, the performance of a SCM that employs a few tens of cells is not a good indicator for the performance of a GCM that can employ billions of grid cells. For the latter, parallel computation overhead and the so-called memory bottle neck are important aspects. ~~Whereas~~ In contrast, for the SCM case, the complete instruction set and solution data can typically be loaded onto the cache memory of a single CPU's

core. Nevertheless, for the readers' reference, the required run times for the different SCM set-ups presented herein are listed in table 1, and figure 3b ~~in Appendix ??~~ also presents quantitative results on this topic and shows that the adaptive-grid solver is well behaved.

Following the turbulence resolving study of Van Hooft et al. (2018), the results presented herein are a proof-of-concept for future 3D modelling, using RANS techniques. The authors of this work realize that the present SCM is a far cry from a complete global model and that more research and development is required before the method can be compared on a global-circulation scale. As shown by e.g. Jablonowski (2004), a 3D adaptive grid also allows a variable grid resolution in the horizontal directions. This further enables the computational resources to focus on the most challenging atmospheric processes where there is a ~~time~~ temporal and spatial variation in the horizontal-resolution requirement of the grid. Examples include the contrasting dynamics between relatively calm centres of high-pressure circulations and those characterizing stormy low-pressure cells. Also, in the case of a sea breeze event ~~(?)~~(Arrillaga et al., 2016), it would be beneficial to temporarily increase the horizontal resolution near the land–sea interface. As such, we encourage the usage of this technique for those meteorologically challenging scenarios.

Acknowledgements. The authors gratefully acknowledge the funding by the ERC Consolidator grant (648666). The LES ensemble results used for the GABLS1 intercomparison are kindly made available by Bob Beare; online via: http://gabls.metoffice.com/.

Competing interests. The authors declare that there are no competing interests.

Code and data availability. Basilisk is a freely available (GPLv3), multi-purpose tool to solve partial differential equations and has it's own website: http://www.basilisk.fr. The code contains solvers for Saint-Venant problems, the Navier-Stokes equations, electrohydrodynamics and more, see http://basilisk.fr/src/README. A selection of examples can be viewed online: http://www.basilisk.fr/src/examples. The website also provides general information including; installation instructions and a tutorial. Furthermore, for the work herein, interested readers can visit the model set-up pages and links to their online locations are presented in table 1. The data can easily be generated by running the scripts. Finally, a snapshot of the used code, as it was used in this the work, is made available via ZENODO, with doi link: https://doi.org/10.5281/zenodo.1203631.

5 ~~The Ekman Spiral~~

~~In this Appendix we validate the numerical solver by evaluating its convergence characteristics for a one dimensional (1D) Ekman-flow set-up. We test both the equidistant-grid and the adaptive-grid approaches. The case describes a neutrally-stratified fluid with kinematic viscosity ν and density ρ in a rotating frame of reference with angular velocity Ω. A flow is forced by a horizontal pressure gradient $\mathrm{d}P/\mathrm{d}y = U_{geo} f \rho$, over a no-slip bottom boundary (located at $z_{bottom} = 0$). Where U_{geo} is a~~

velocity scale that is also known as the geostrophic wind. There exists an analytical, 1D, steady solution for the horizontal wind components (u_E,v_E), that is known as the Ekman spiral;

$$u_E = U_{geo}\left(1 - e^{-\gamma z}\cos(\gamma z)\right),$$

$$v_E = U_{geo} e^{-\gamma z}\sin(\gamma z),$$

with γ the so-called Ekman depth, $\gamma = \sqrt{\Omega/\nu}$. We initialize our model and set boundary conditions consistent with Eqs 17 and 18. Using a domain height of $L = 100\gamma$. The error (η) in the numerically obtained solution (u^n, v^n) is evaluated as,

$$\eta = \int_{z_{bottom}}^{z_{top}} \|u^n - u_E\| + \|v^n - v_E\| \mathrm{d}z,$$

at the end of the run that is performed until $t_{end} = 10 \times \gamma/U_{geo}$, with a timestep $\Delta t = 0.01 \times \gamma/U_{geo}$. We study the spatial-convergence properties of the fixed-grid solver and the adaptive-grid approach by iteratively decreasing the (maximum) grid size. For the adaptive-grid solver we decrease the refinement criteria ζ for the velocity components accordingly[2]. In order to facilate a comparison between the methods, we diagnose the used cells for the adaptive grid run. Figure 3 a shows that both approaches are second-order accurate. Were the adaptive grid results are more accurate than the results from the fixed-grid approach, employing the same number of grid cells. Figure 3 b shows that for both approaches the required effort (i.e. in wall-clock time) scales linearly with the number of grid cells, except for the runs that require less than one-tenth of a second to perform. This plots reveals that *per grid cell* there is computational overhead for the adaptive-grid approach. The results in this appendix show that the used numerical methods are well behaved.

[2] The details of the exact case set-up can be found online:

References

Arrillaga, J. A., Yagüe, C., Sastre, M., and Román-Cascón, C.: A characterisation of sea-breeze events in the eastern Cantabrian coast (Spain) from observational data and WRF simulations, Atmospheric Research, 181, 265–280, 2016.

Baas, P., van de Wiel, B., van der Linden, S., and Bosveld, F.: From Near-Neutral to Strongly Stratified: Adequately Modelling the Clear-Sky Nocturnal Boundary Layer at Cabauw, Boundary-Layer Meteorology, pp. 1–22, 2017.

Beare, R. J., Macvean, M. K., Holtslag, A. A., Cuxart, J., Esau, I., Golaz, J.-C., Jimenez, M. A., Khairoutdinov, M., Kosovic, B., Lewellen, D., et al.: An intercomparison of large-eddy simulations of the stable boundary layer, Boundary-Layer Meteorology, 118, 247–272, 2006.

Beetham, E., Kench, P. S., O'Callaghan, J., and Popinet, S.: Wave transformation and shoreline water level on Funafuti Atoll, Tuvalu, Journal of Geophysical Research: Oceans, 121, 311–326, 2016.

Beljaars, A. C. M., Holtslag, A., and Van Westrhenen, R.: Description of a software library for the calculation of surface fluxes, KNMI De Bilt, Netherlands, 1989.

Bosveld, F. C., Baas, P., Steeneveld, G.-J., Holtslag, A. A., Angevine, W. M., Bazile, E., de Bruijn, E. I., Deacu, D., Edwards, J. M., Ek, M., et al.: The third GABLS intercomparison case for evaluation studies of boundary-layer models. Part B: results and process understanding, Boundary-layer meteorology, 152, 157–187, 2014.

Cuxart, J., Holtslag, A. A., Beare, R. J., Bazile, E., Beljaars, A., Cheng, A., Conangla, L., Ek, M., Freedman, F., Hamdi, R., et al.: Single-column model intercomparison for a stably stratified atmospheric boundary layer, Boundary-Layer Meteorology, 118, 273–303, 2006.

Dunbar, T., Hanert, E., and Hogan, R.: A one-dimensional finite-element boundary-layer model with a vertical adaptive grid, Boundary-layer meteorology, 128, 459–472, 2008.

Eggers, J., Grava, T., Herrada, M., and Pitton, G.: Spatial structure of shock formation, Journal of Fluid Mechanics, 820, 208–231, 2017.

England, D. E. and McNider, R. T.: Stability functions based upon shear functions, Boundary-Layer Meteorology, 74, 113–130, 1995.

Grell, G. A., Peckham, S. E., Schmitz, R., McKeen, S. A., Frost, G., Skamarock, W. C., and Eder, B.: Fully coupled "online" chemistry within the WRF model, Atmospheric Environment, 39, 6957–6975, 2005.

Holtslag, A. and Boville, B.: Local versus nonlocal boundary-layer diffusion in a global climate model, Journal of Climate, 6, 1825–1842, 1993.

Holtslag, A., Svensson, G., Baas, P., Basu, S., Beare, B., Beljaars, A., Bosveld, F., Cuxart, J., Lindvall, J., Steeneveld, G., et al.: Stable atmospheric boundary layers and diurnal cycles: challenges for weather and climate models, Bulletin of the American Meteorological Society, 94, 1691–1706, 2013.

Howland, C. J., Antkowiak, A., Castrejón-Pita, J. R., Howison, S. D., Oliver, J. M., Style, R. W., and Castrejón-Pita, A. A.: It's Harder to Splash on Soft Solids, Physical review letters, 117, 184 502, 2016.

Jablonowski, C.: Adaptive grids in weather and climate modeling, Ph.D. thesis, University of Michigan, 2004.

Jablonowski, C., Oehmke, R. C., and Stout, Q. F.: Block-structured adaptive meshes and reduced grids for atmospheric general circulation models, Philosophical Transactions of the Royal Society of London A: Mathematical, Physical and Engineering Sciences, 367, 4497–4522, 2009.

Kirstetter, G., Hu, J., Delestre, O., Darboux, F., Lagrée, P.-Y., Popinet, S., Fullana, J.-M., and Josserand, C.: Modeling rain-driven overland flow: Empirical versus analytical friction terms in the shallow water approximation, Journal of Hydrology, 536, 1–9, 2016.

Kosović, B. and Curry, J. A.: A large eddy simulation study of a quasi-steady, stably stratified atmospheric boundary layer, Journal of the atmospheric sciences, 57, 1052–1068, 2000.

Kumar, V., Svensson, G., Holtslag, A., Meneveau, C., and Parlange, M. B.: Impact of surface flux formulations and geostrophic forcing on large-eddy simulations of diurnal atmospheric boundary layer flow, Journal of Applied Meteorology and Climatology, 49, 1496–1516, 2010.

Lenderink, G. and Holtslag, A. A.: An updated length-scale formulation for turbulent mixing in clear and cloudy boundary layers, Quarterly Journal of the Royal Meteorological Society, 130, 3405–3427, 2004.

Louis, J.: A short history of PBL parameterization at ECMWF, in: paper presented at the Workshop on Planetary Boundary Layer Parameterization, Eur. Cent. For Medium-Range Weather Forecasts, Reading, England, 1982, 1982.

Marivela-Colmenarejo, R.: Numerical Perspective on Tsunami Hazards and Their Mitigation by Coastal Vegetation, Ph.D. thesis, Virginia Tech, 2017.

Mellor, G. L. and Yamada, T.: Development of a turbulence closure model for geophysical fluid problems, Reviews of Geophysics, 20, 851–875, 1982.

Neggers, R. A., Siebesma, A. P., and Heus, T.: Continuous single-column model evaluation at a permanent meteorological supersite, Bulletin of the American Meteorological Society, 93, 1389–1400, 2012.

Popinet, S.: Quadtree-adaptive tsunami modelling, Ocean Dynamics, 61, 1261–1285, 2011.

Popinet, S.: Time-implicit discretisation of reaction–diffusion equations, http://www.basilisk.fr/src/diffusion.h, accessed: 2018-01-01, 2017a.

Popinet, S.: Multigrid Poisson-Helmholtz solvers, http://www.basilisk.fr/src/poisson.h, accessed: 2018-01-01, 2017b.

Poulos, G. S., Blumen, W., Fritts, D. C., Lundquist, J. K., Sun, J., Burns, S. P., Nappo, C., Banta, R., Newsom, R., Cuxart, J., et al.: CASES-99: A comprehensive investigation of the stable nocturnal boundary layer, Bulletin of the American Meteorological Society, 83, 555–581, 2002.

Reynolds, O.: On the dynamical theory of incompressible viscous fluids and the determination of the criterion., Philosophical transacations of the Royal Society of London, 56, 40–45, 1895.

Rohatgi, A.: WebPlotDigitizer, https://github.com/ankitrohatgi/WebPlotDigitizer, accessed via the web interface: 2018-01-01, 2018.

Schaller, R. R.: Moore's law: past, present and future, IEEE spectrum, 34, 52–59, 1997.

Slingo, J.: The development and verification of a cloud prediction scheme for the ECMWF model, Quarterly Journal of the Royal Meteorological Society, 113, 899–927, 1987.

St-Cyr, A., Jablonowski, C., Dennis, J. M., Tufo, H. M., and Thomas, S. J.: A comparison of two shallow-water models with nonconforming adaptive grids, Monthly Weather Review, 136, 1898–1922, 2008.

Stull, R. B.: An introduction to boundary layer meteorology, vol. 1, Springer Science & Business Media, 670 pp, 1988.

Svensson, G., Holtslag, A., Kumar, V., Mauritsen, T., Steeneveld, G., Angevine, W., Bazile, E., Beljaars, A., De Bruijn, E., Cheng, A., et al.: Evaluation of the diurnal cycle in the atmospheric boundary layer over land as represented by a variety of single-column models: the second GABLS experiment, Boundary-Layer Meteorology, 140, 177–206, 2011.

Van Hooft, J. A., Popinet, S., Van Heerwaarden, C. C., Van der Linden, S. J. A., de Roode, S. R., and Van de Wiel, B. J. H.: Towards Adaptive Grids for Atmospheric Boundary Layer Simulations, Boundary-Layer Meteorology, 167, 421–443, 2018.

Wyant, M. C., Bretherton, C. S., Chlond, A., Griffin, B. M., Kitagawa, H., Lappen, C.-L., Larson, V. E., Lock, A., Park, S., De Roode, S. R., et al.: A single-column model intercomparison of a heavily drizzling stratocumulus-topped boundary layer, Journal of Geophysical Research: Atmospheres, 112, 2007.

Zhou, Y., Lagrée, P.-Y., Popinet, S., Ruyer, P., and Aussillous, P.: Experiments on, and discrete and continuum simulations of, the discharge of granular media from silos with a lateral orifice, Journal of Fluid Mechanics, 829, 459–485, 2017.

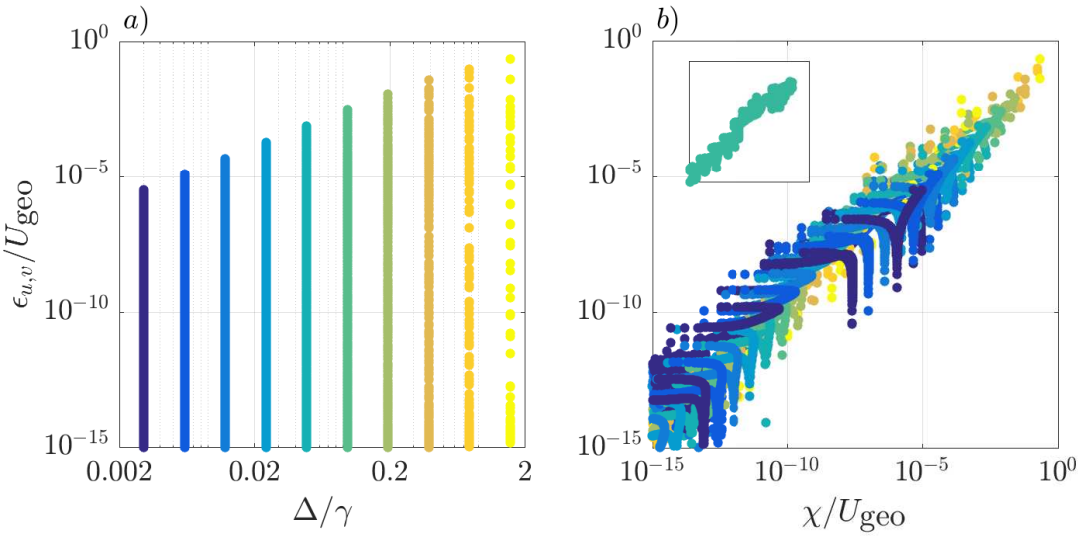

Figure 1. The locally evaluated error in the numerical solutions for u and v based on the analytical solution ($\epsilon_{u,v}$, see Eq. 19) for 10 runs with equidistant grids with different mesh-element sizes. The left-hand side plot (a) Shows that the diagnosed errors for each run plotted against the used mesh-element size (Δ). The right-hand side plot (b) shows, with the same colour coding as in the left-hand side plot (a), the correlation between the wavelet-based estimated error (χ) and the corresponding diagnosed error in the numerically obtained solution (ϵ). The inset (using the same axis scales) shows the results for a single run, and reveal a spread of serval orders of magnitude in both ϵ and χ values.

Table 1. The exact formulation of the methods are described at the online locations of the definition files for the different cases presented in this manuscript.

Section	Case	Grid	URL: http://www.basilisk.fr...	~~Solver timesteps~~ Number of time steps	Wall
~~3.1~~ 3.1	~~GABLS1~~ Ekman spiral	Adaptive	/sandbox/Antoonvh/ekman.c	~~14404~~ 1000 ($\times$20 runs)	$\approx$ ~~1.~~
"	"	Fixed & Equidistant	/sandbox/Antoonvh/ekmanfg.c	~~14404~~ 1000 ($\times$10 runs)	$\approx$ ~~0.~~
~~3.2~~3.2	~~GABLS2~~ GABLS1	Adaptive	/sandbox/Antoonvh/GABLS1.c	~~24262~~ 14404	$\approx$ ~~9~~
"	"	Fixed & Equidistant	/sandbox/Antoonvh/GABLS1fg.c	~~33993~~ 14404	$\approx$ ~~22~~
~~Appendix~~3.3	~~Ekman spiral~~ GABLS2	Adaptive	/sandbox/Antoonvh/GABLS2.c	~~1000 ($\times$20 runs)~~24262	$\approx$ ~~19~~
"	"	Fixed & Equidistant	/sandbox/Antoonvh/GABLS2fg.c	~~1000 ($\times$10 runs)~~33993	$\approx$ ~~18~~

The wall-clock times are evaluated using a single core (processor model: Intel i7-6700 HQ).

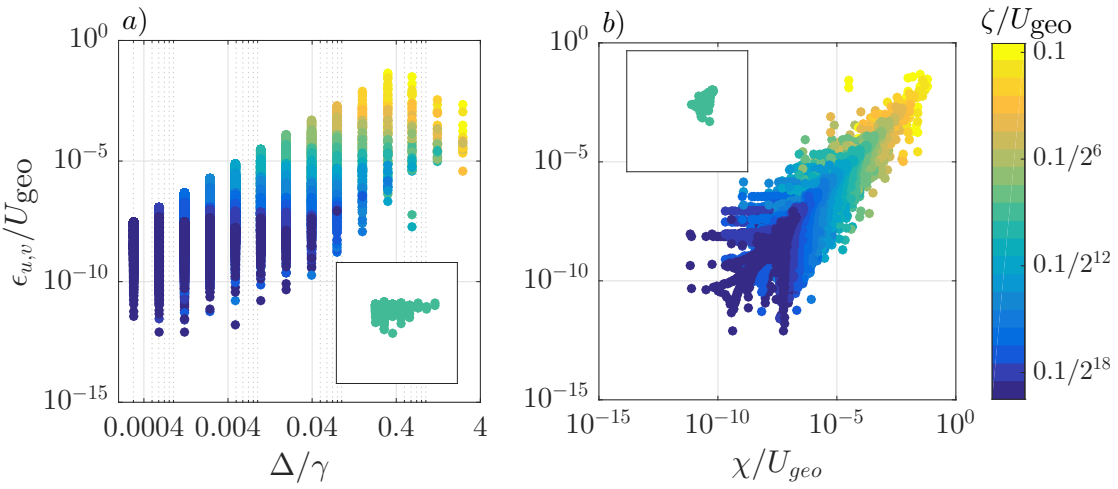

Figure 2. The locally evaluated error in the numerical solutions for u and v based on the analytical solution ($\epsilon_{u,v}$, see Eq. 19) for 20 runs using the adaptive-grid approach with different refinement criteria (see colourbar). The left-hand side plot (a) Shows that the diagnosed errors for each run plotted against the used mesh-element size (Δ). The inset (using the same axis scales) shows the results for a single run. The right-hand side plot (b) shows the correlation between the wavelet-based estimated error (χ) and the corresponding diagnosed error in the numerically obtained solution (ϵ)). The inset (using the same axis scales) shows the results for a single run, and reveals a relatively small spread in both ϵ and χ values compared to the equidistant-grid results presented in figure 1b.

~~The scaling characteristics for the laminar-Ekman-spiral case. (a) Presents the error convergence for the equidistant-grid and adaptive-grid approach, showing that the solver is second-order accurate. The wall-clock time for the different runs is presented in (b), showing that for both of the aforementioned approaches, the required effort scales linearly with the number of grid cells.~~

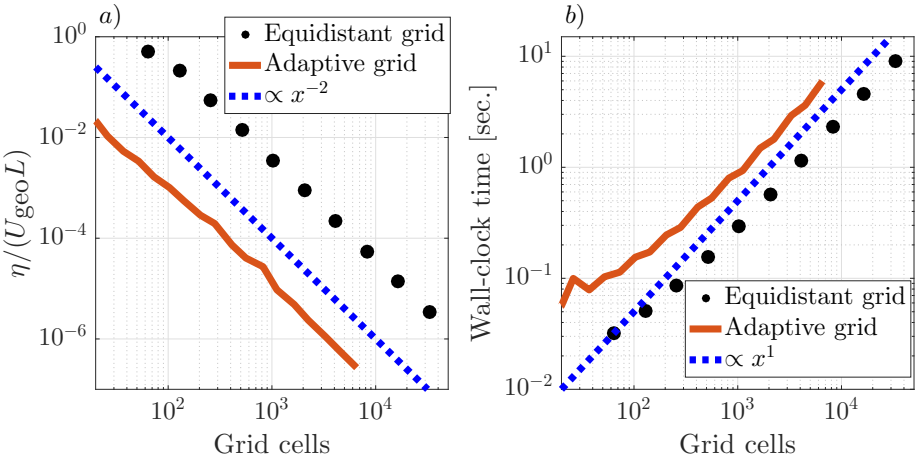

Figure 3. The scaling characteristics for the laminar-Ekman-spiral case. (a) Presents the error convergence for the equidistant-grid and adaptive-grid approach. The errors (η) follow the slope of the blue dashed line that indicates the second-order accuracy of the methods. The wall-clock time for the different runs is presented in (b), showing that for both of the aforementioned approaches, the required effort scales linearly with the number of grid cells.

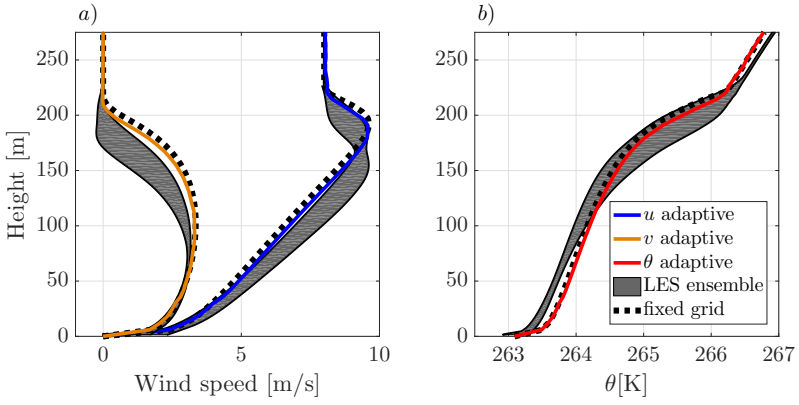

Figure 4. Time averaged profiles over the eight hour of the run according to the GABLS1 intercomparison scenario. For (a) the horizontal wind components and (b) the potential temperature. Results are obtained with the present adaptive-grid SCM (coloured lines), the LES models ensemble (i.e $\mathrm{mean} \pm \sigma$) from Beare et al. (2006) (grey-shaded areas) and the present SCM, employing an equidistant and static grid with a 6.25 meter resolution (dashed lines).

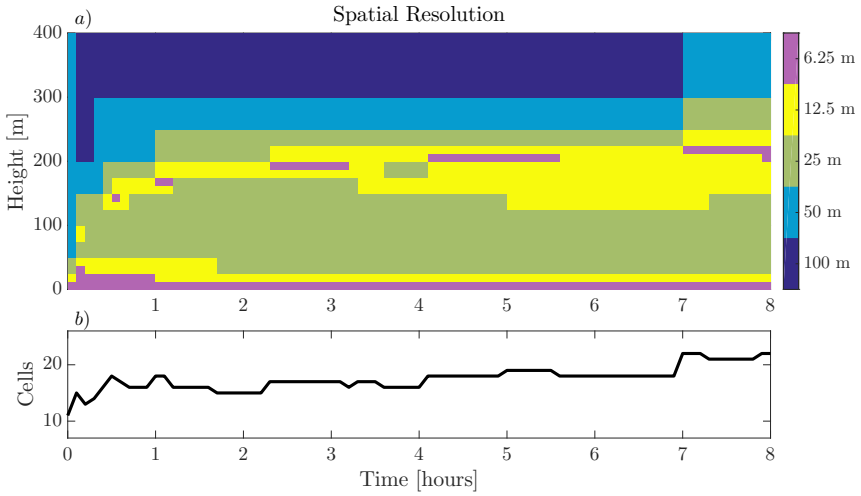

Figure 5. Evolution of (a) the vertical spatial-resolution distribution and (b) the total number of grid cells, for the GABLS1 intercomparison case.

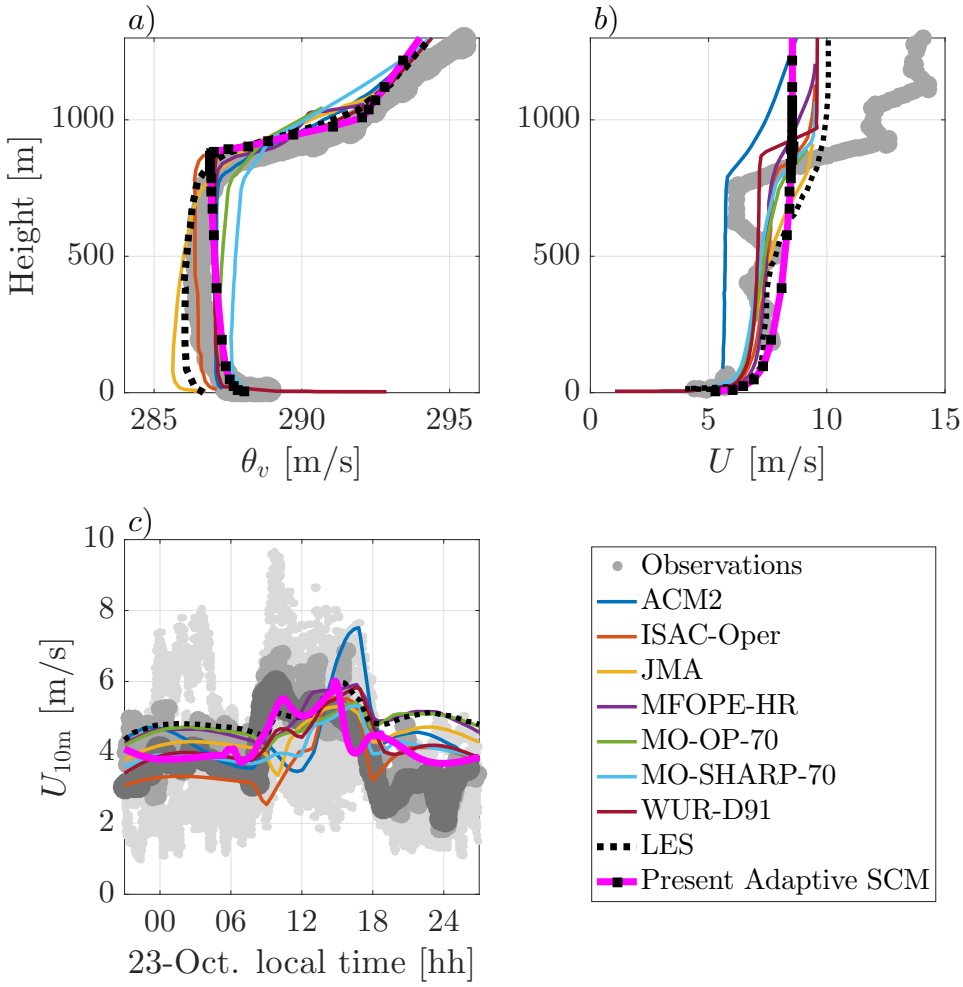

Figure 6. Intercomparison of the results obtained with the adaptive-grid SCM and the participating models in the work of (Svensson et al., 2011) for the vertical profiles of (a) the virtual potential temperature and (b) the wind-speed magnitude. Lower panel: (c) the evolution of the 10-meter wind speed (U_{10m}) on the ~~22-th~~ 23-th of October. For the used model abbreviations in the legend, see Svensson et al. (2011). The different shades of grey in plot c) indicate observations from different meassurement devices, see Svensson et al. (2011) for the details.

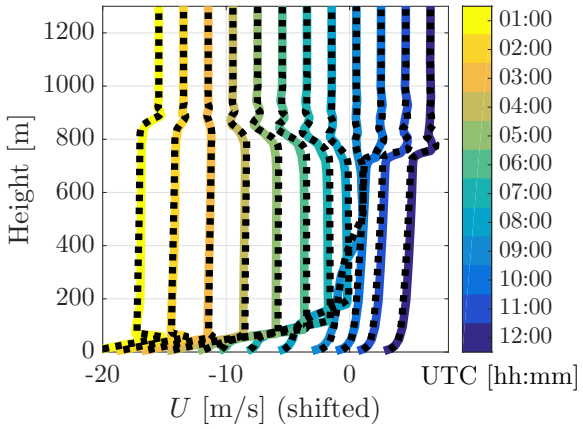

Figure 7. Vertical profiles of the wind-speed magnitude U obtained with the adaptive-grid (in colour) and the fixed equidistant-grid (dashed) SCMs. The twelve plotted profiles are obtained for the ~~23-th~~ 24-th of October with an hourly interval, starting from 1:00 AM local time. Noting that the profiles are shifted in order to distinguish between the different times (with vanishing wind at the surface).

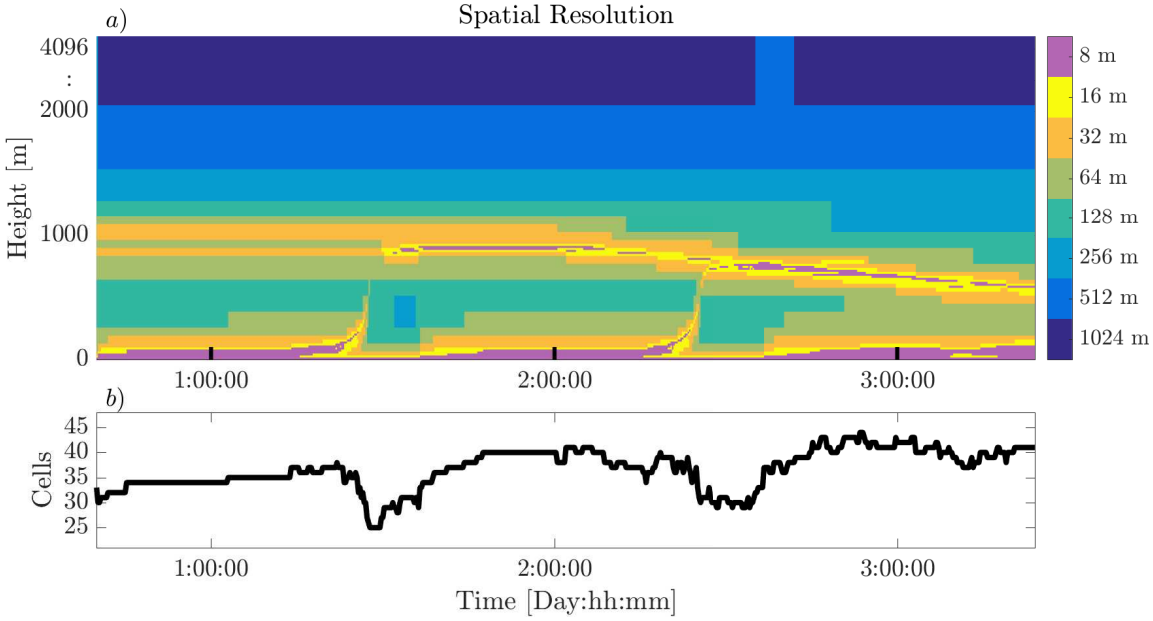

Figure 8. Evolution of (a) the vertical spatial resolution and (b) the total number of grid cells, for the GABLS2 intercomparison case. Two full diurnal cycles, corresponding to the 23-rd and 24-th day of October, 1999 (ranging from the labels 1:00:00 to 3:00:00 on the x-axis).